

PAPER • OPEN ACCESS

First experimental exploration of real-time cardiorespiratory motion management for future stereotactic arrhythmia radioablation treatments on the MR-linac

To cite this article: O Akdag *et al* 2022 *Phys. Med. Biol.* **67** 065003

View the [article online](#) for updates and enhancements.

You may also like

- [MR-based cardiac and respiratory motion correction of PET: application to static and dynamic cardiac \$^{18}\text{F}\$ -FDG imaging](#)
Y Petibon, T Sun, P K Han *et al.*
- [Cardiorespiratory coupling in young healthy subjects](#)
Tomasz Sobiech, Teodor Buchner, Pawe Krzesiski *et al.*
- [Technical aspects of cardiorespiratory estimation using subspace projections and cross entropy](#)
John Morales, Jonathan Moeyersons, Dries Testelmans *et al.*

New Webinar Collection
IN ADVANCED RADIOTHERAPY AND MEDICAL IMAGING QA

[VIEW RECORDINGS](#)

END-to-END QA with the QUASAR™ MP Body Phantom
Gamma Knife® Image Distortion Analysis with the QUASAR™ GRID3D
Measuring Geometric Distortion with Sub-Millimeter Accuracy

MODUS QA



PAPER

OPEN ACCESS






RECEIVED
18 October 2021REVISED
11 February 2022ACCEPTED FOR PUBLICATION
21 February 2022PUBLISHED
9 March 2022

Original content from this work may be used under the terms of the [Creative Commons Attribution 4.0 licence](#).

Any further distribution of this work must maintain attribution to the author(s) and the title of the work, journal citation and DOI.



First experimental exploration of real-time cardiorespiratory motion management for future stereotactic arrhythmia radioablation treatments on the MR-linac

O Akdag^{1,*} , P T S Borman¹ , P Woodhead^{1,2}, P Uijtewaal¹, S Mandija^{1,3} , B Van Asselen¹, J J C Verhoeff¹ , B W Raaymakers¹ and M F Fast¹ 

¹ Department of Radiotherapy, University Medical Center Utrecht, Heidelberglaan 100, 3584 CX Utrecht, The Netherlands

² Elekta AB, Kungstensgatan 18, 113 57 Stockholm, Sweden

³ Computational Imaging Group for MR Diagnostics and Therapy, Center for Image Sciences, University Medical Center Utrecht, Heidelberglaan 100, 3584 CX Utrecht, The Netherlands

* Author to whom any correspondence should be addressed.

E-mail: o.akdag-3@umcutrecht.nl and m.f.fast-2@umcutrecht.nl

Keywords: stereotactic arrhythmia radioablation, ventricular tachycardia, MR-linac, MRI-guided radiotherapy, cardiorespiratory motion management, gating, MLC-tracking

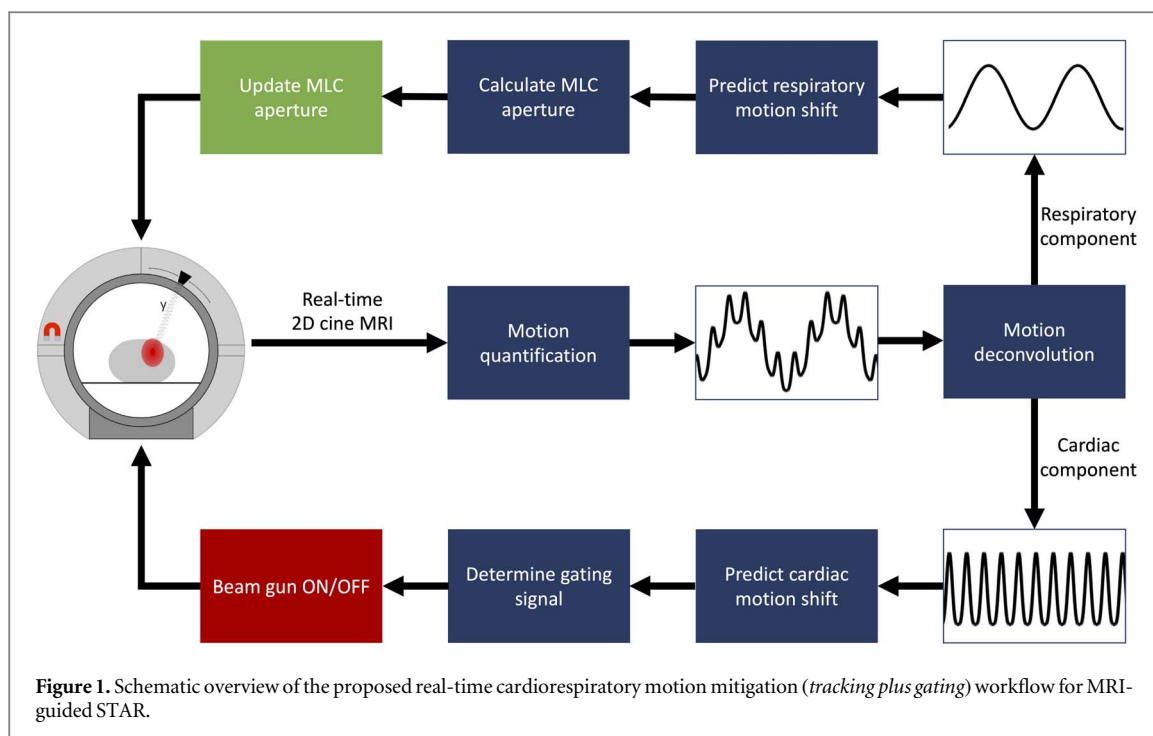
Supplementary material for this article is available [online](#)

Abstract

Objective. Stereotactic arrhythmia radioablation (STAR) is a novel, non-invasive treatment for refractory ventricular tachycardia (VT). The VT isthmus is subject to both respiratory and cardiac motion. Rapid cardiac motion presents a unique challenge. In this study, we provide first experimental evidence for real-time cardiorespiratory motion-mitigated MRI-guided STAR on the 1.5 T Unity MR-linac (Elekta AB, Stockholm, Sweden) aimed at simultaneously compensating cardiac and respiratory motions. **Approach.** A real-time cardiorespiratory motion-mitigated radiotherapy workflow was developed on the Unity MR-linac in research mode. A 15-beam intensity-modulated radiation therapy treatment plan (1 × 25 Gy) was created in Monaco v.5.40.01 (Elekta AB) for the Quasar MRI^{4D} phantom (ModusQA, London, ON). A film dosimetry insert was moved by combining either artificial (cos⁴, 70 bpm, 10 mm peak-to-peak) or subject-derived (59 average bpm, 15.3 mm peak-to-peak) cardiac motion with respiratory (sin, 12 bpm, 20 mm peak-to-peak) motion. A balanced 2D cine MRI sequence (13 Hz, field-of-view = 400 × 207 mm², resolution = 3 × 3 × 15 mm³) was developed to estimate cardiorespiratory motion. Cardiorespiratory motion was estimated by rigid registration and then deconvoluted into cardiac and respiratory components. For beam gating, the cardiac component was used, whereas the respiratory component was used for MLC-tracking. In-silico dose accumulation experiments were performed on three patient data sets to simulate the dosimetric effect of cardiac motion on VT targets. **Main results.** Experimentally, a duty cycle of 57% was achieved when simultaneously applying respiratory MLC-tracking and cardiac gating. Using film, excellent agreement was observed compared to a static reference delivery, resulting in a 1%/1 mm gamma pass rate of 99%. The end-to-end gating latency was 126 ms on the Unity MR-linac. Simulations showed that cardiac motion decreased the target's D98% dose between 0.1 and 1.3 Gy, with gating providing effective mitigation. **Significance.** Real-time MRI-guided cardiorespiratory motion management greatly reduces motion-induced dosimetric uncertainty and warrants further research and development for potential future use in STAR.

1. Introduction

Ventricular tachycardia (VT) is a severe cardiac arrhythmia condition, which is a major risk factor for sudden cardiac death. The heterogeneous zone of intertwined healthy and scarred cardiac tissue surrounding a



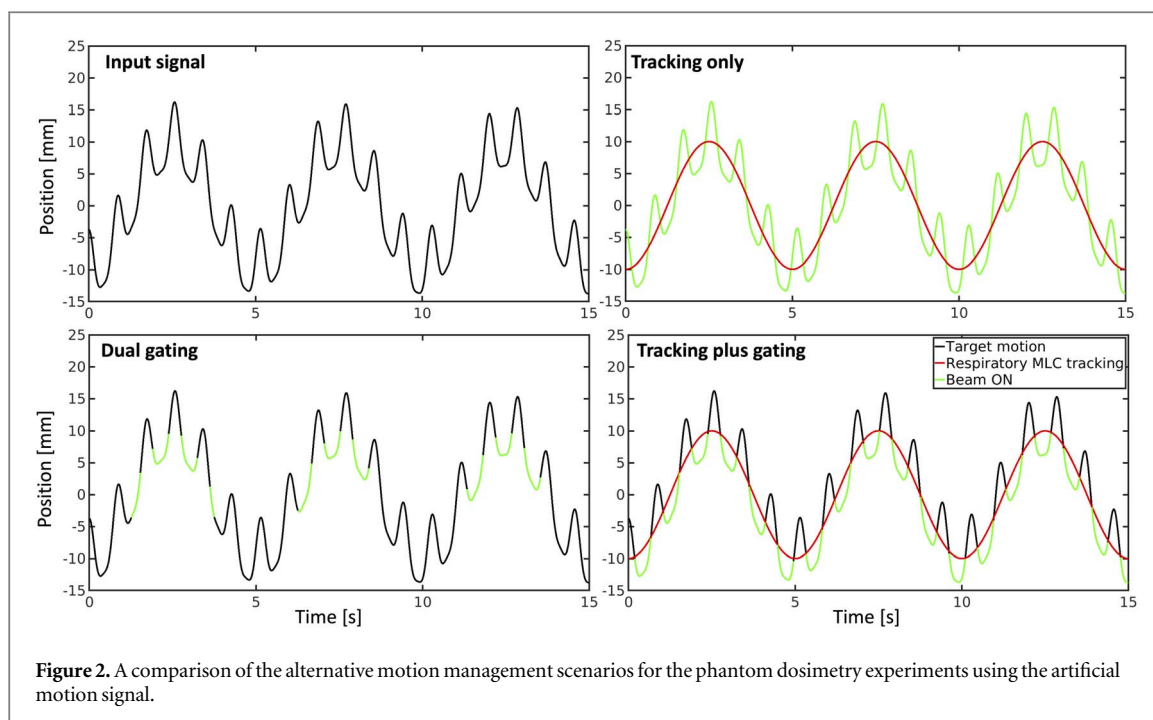
myocardial scar in the ventricles can be the source of abnormal electrical activity causing VT. VT is mainly managed by providing antiarrhythmic drugs or placing an implantable cardioverter defibrillator (Liu *et al* 2019). In addition, minimal invasive endocardial catheter ablation is the clinical standard of care. This treatment strategy aims to ablate the arrhythmogenic substrate responsible for VT. The catheter ablation procedure comes with risks, which can lead to complications and death (Calkins *et al* 2000, Marchlinski *et al* 2000, Soejima *et al* 2001, Aliot *et al* 2009).

Recently, a novel non-invasive stereotactic arrhythmia radioablation (STAR) or cardiac radioablation (CR) technique has emerged as salvage treatment for refractory VT patients (Cuculich *et al* 2017, Zei and Soltys 2017, Robinson *et al* 2019, van der Ree *et al* 2020). STAR is a stereotactic body radiotherapy (SBRT) treatment procedure in which a single high dose of radiation (typically 1×25 Gy) is delivered to the VT substrate. In first patient studies, STAR has proven highly effective at reducing the VT burden with few reported (acute) toxicities (Robinson *et al* 2019, Sharp *et al* 2019). STAR is especially promising for patients who are either not eligible for (another) catheter ablation or where previous ablation procedures failed (Cvek *et al* 2014, Scholz *et al* 2019). However, as (parts of) the heart and adjacent mediastinal organs-at-risk (OARs) are highly radiation sensitive, keeping the treatment volume to a minimum is crucial.

Reducing STAR treatment volumes is uniquely challenging due to cardiac and respiratory motion-induced position uncertainties of the target. Currently, the target position uncertainties during treatment are either accounted for by respiratory motion management or by increased planning target volume (PTV) margins (Lydiard *et al* 2021). To minimize the toxicity risk during STAR, proactive cardiorespiratory motion management might be beneficial. Respiratory motion management is widely applied in radiotherapy (Keall *et al* 2006), while cardiac motion remains a unique challenge due to its complexity and rapid periodicity. However, cardiac motion mitigation techniques are widely applied in the cardiovascular MRI (CMR) domain (Lee *et al* 2019, Curtis and Cheng 2020, Kramer *et al* 2020).

Until now, STAR treatments were primarily done on C-arm or robotic (e.g. CyberKnife) linacs. These devices are able to perform STAR, while mitigating for respiratory motion using either an ITV approach, gating or tracking (Lydiard *et al* 2021). Accurate visualization of the target is challenging due to contrast limitations of x-ray guidance. A recent case study was published, in which respiratory-gated STAR was performed with MRI-guidance based on extra-cardiac structures (e.g. liver dome, diaphragm and esophagus) on the MR-linac (Mayinger *et al* 2020).

In this study, we develop a prototype MRI-guided STAR workflow for the 1.5 T Unity MR-linac (Elekta AB, Stockholm, Sweden) with active cardiorespiratory motion mitigation inspired by techniques from CMR and radiotherapy. To this end, we demonstrate a real-time adaptive MRI-guided dose delivery approach in which the radiation delivery is gated to a pre-defined cardiac phase, while simultaneously performing respiratory motion tracking with the multi-leaf collimator (MLC). The proposed online MRI-guided dose delivery approach is first



explored in an experimental phantom setup, while the dosimetric effects of cardiac motion within STAR patients is then estimated using Monte Carlo simulations.

2. Material and methods

2.1. Experimental setup on the MR-linac

Figure 1 provides a schematic overview of the proposed cardiorespiratory motion mitigation workflow on the MR-linac. The individual steps of the workflow are explained in more detail in the following subsections. In short, A Quasar MRI^{4D} motion phantom (ModusQA Inc., London, ON, Canada) was placed in the bore for film dosimetry experiments. The phantom contained a moving spherical object that was considered the treatment target. Real-time 2D cine MRI of the target were continuously streamed for motion quantification. Prospective Kalman filtering was performed to deconvolute the obtained motion signal into cardiac and respiratory motion components. A linear (ridge) predictor model was used to predict the cardiac and respiratory motion signals as a means to compensate for system latencies. The predicted respiratory motion component was used as input for MLC-tracking, while the predicted cardiac component was used for cardiac gated radiation delivery with the cardiac midposition as gating threshold (figure 1). For the remainder of this manuscript, this scenario is referred to as the *tracking plus gating* approach. A research interface was used to facilitate real-time MLC-tracking and gating on the 1.5 T Unity MR-linac. For MLC-tracking, updated MLC apertures were transferred to the MLC, while for gating the pulse-repetition frequency of the linac was modulated.

2.1.1. Alternative motion management scenarios

Alternative motion mitigated dose delivery scenarios were created for comparison. First, cardiac motion mitigation was omitted to investigate the dosimetric effects of cardiac motion on the dose delivery. Here, only respiratory MLC-tracking was used with respiratory motion prediction (*tracking-only*). Second, cardiac and respiratory motion were simultaneously mitigated by gating. The respiratory midposition was used as gating threshold for the respiratory motion component. Irradiation would therefore only be done when the cardiac and respiratory gating windows overlap (*dual gating*). Third, cardiac motion prediction was omitted for cardiac gated beam delivery to investigate the effects of the system latencies. Respiratory motion prediction for MLC-tracking was maintained (*tracking plus gating without cardiac motion prediction*).

An overview of the delivery scenarios with the corresponding artificial motion pattern is shown in figure 2. The overview of the delivery scenarios with the corresponding subject-derived motion pattern (Akdag et al 2021) is depicted in figure S1 in the supplement available online at stacks.iop.org/PMB/67/065003/mmedia. All experiments were performed twice and averaged to decrease measurement uncertainties.

2.1.2. Motion phantom

The Quasar MRI^{4D} phantom consisted of a water-filled body oval with a movable cylinder insert. This cylinder was filled with a MnCl₂-doped agarose gel and contained a spherical treatment target of 3 cm in diameter, intersected with a thin film cassette insert in the coronal plane. Radiochromic film was inserted for dosimetric experiments. Two different 1D cardiorespiratory motion patterns were defined mimicking cranio-caudal (CC) physiological motion of a treatment target in the left ventricle. For the first motion pattern, the cardiac motion component was defined as periodic motion (cos⁴, 70 bpm, 10 mm peak-to-peak). For the second motion pattern, a subject-derived cardiac motion component (59 bpm, 15.3 mm peak-to-peak in CC direction) was used. This cardiac motion component was obtained using an *in vivo* balanced steady state free precession (bSSFP) real-time 2D cine CMR sequence (TR/TE = 2.3/1.1 ms, flip angle = 48°, field-of-view = 300 × 300 mm², resolution = 2.8 × 2.8 × 10 mm³, Partial Fourier factor = 0.625, Compressed SENSE = 3.5, temporal resolution = 71 ms) in a healthy volunteer (Akdag *et al* 2021). The cardiorespiratory motion patterns were then obtained by combining each of the cardiac motion components with a respiratory motion component, which was simulated as periodic motion (sin, 12 bpm, 20 mm peak-to-peak).

2.1.3. Real-time MR-guided cardiorespiratory motion estimation

A balanced 2D cine MRI (TR/TE = 3/1.48 ms, flip angle = 48°, SENSE = 1.5, field-of-view = 400 × 207 mm², resolution = 3 × 3 × 15 mm³, Partial Fourier factor = 0.65) sequence was used to allow imaging with a frequency of 13 Hz. The acquired MR images were continuously streamed and processed using in-house developed C++ software. The position of the target was estimated using 1D normalized cross-correlation with respect to a pre-beam reference image. Prospective linear Kalman filtering was performed to deconvolute the obtained position signal into cardiac and respiratory motion components in real-time (Spincemaille *et al* 2008). After deconvolution of the motion signal, lookahead prediction was independently applied to the cardiac and respiratory motion components to compensate for system latencies (see section 2.1.4).

2.1.4. System latencies

The proposed workflow for real-time cardiorespiratory motion mitigation (see figure 1) is subject to system latencies. End-to-end system latency is defined as the time difference between the occurrence of a physical event (phantom motion) and the reaction of the system to act on that event (adjusting the MLC aperture for tracking and/or gating the radiation delivery). The contributors to the system latency are the time between the acquisition of the k-space center and receiving the image (T_{signal}), the image processing time for motion quantification (T_{proc}), the adjustment of the MLC aperture (T_{MLC}) or the necessary time for the beam to be turned on/off (T_{gate}) (Borman *et al* 2018, Uijtewaal *et al* 2021). The latency of MLC-tracking system can then be defined as:

$$\tau_{\text{MLC}} = T_{\text{signal}} + T_{\text{proc}} + T_{\text{MLC}}. \quad (1)$$

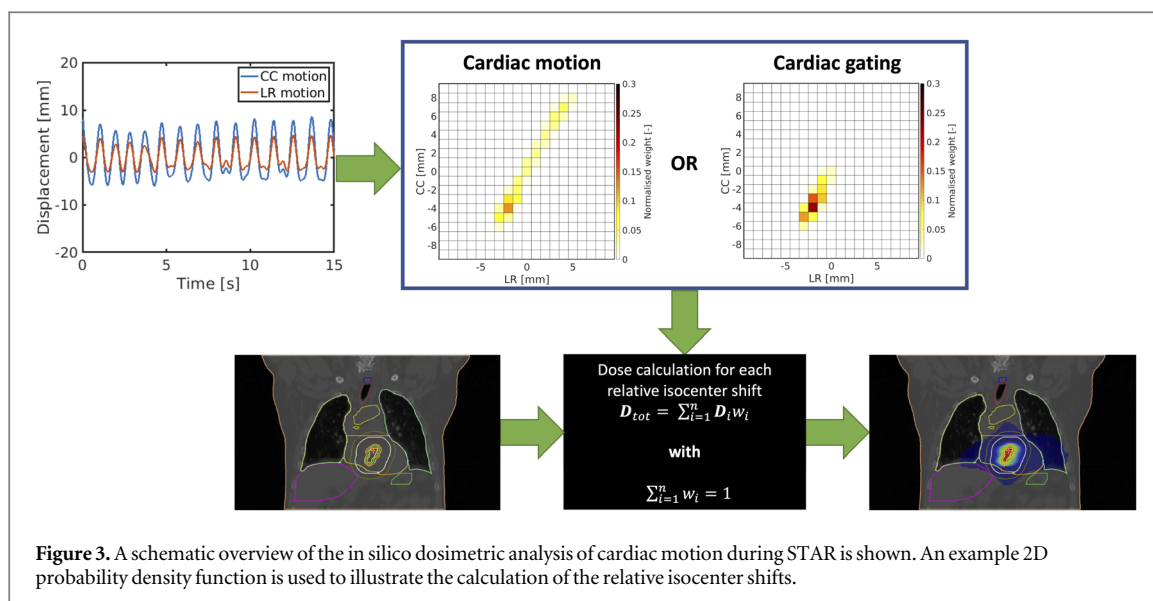
τ_{MLC} was estimated using the on-board EPID panel (Uijtewaal *et al* 2021). Similarly, the gating system latency is defined as:

$$\tau_{\text{gate}} = T_{\text{signal}} + T_{\text{proc}} + T_{\text{gate}}. \quad (2)$$

T_{gate} was estimated by measuring the time delay between sending a beam on/off signal and the starting/stopping of the gun trigger pulses into the triode gun. Pulse timings were measured by routing them through a Raspberry Pi computer mounted on the MR-linac gantry. T_{signal} and T_{proc} were measured by comparing the phantom's reference positions with the streamed images and logging the processing times (Uijtewaal *et al* 2021).

2.1.5. Linear predictor modeling

Both system latencies were compensated by using a linear (ridge) regression model (Krauss *et al* 2011). This model was previously applied to predict respiratory motion (Uijtewaal *et al* 2021). We used two instances of this prediction model to predict both the cardiac and respiratory motion components in parallel with a training time of 60 s. For gated radiation delivery, the motion components were predicted at 166 and 249 ms ahead. For respiratory MLC-tracking, the respiratory motion component was predicted at 166 and 332 ms ahead. The current system latency was continuously calculated based on the age of the last received position. Depending on the current system latency, the desired position of the target could be determined by interpolation. The accuracy of the total motion, cardiac motion and respiratory motion signal determination, which were used for cardiorespiratory motion mitigation, was then analysed by calculating the mean absolute error (MAE) and root-mean-square error (RMSE) with respect to the corresponding phantom input.



2.1.6. Dosimetry experiments

A 15-beam intensity-modulated radiation therapy (IMRT) treatment plan (1×25 Gy) for the Unity MR-linac was created in Monaco v.5.40.01, by adapting our clinical planning template for MRI-guided ultracentral lung SBRT to STAR. A 5 mm isotropic PTV margin was used. Film dosimetry experiments were conducted as a means to test the performance of the proposed MR-guided cardiorespiratory motion-mitigated dose delivery workflow. For these experiments GafchromicTM EBT3 and EBT-XD (Ashland Advanced Materials, Bridgewater NJ, USA) dosimetric films were used. To best fit the optimal dynamic range of the film and to limit overall measurement time (given the maximum dose rate of 425 MU min^{-1}), the prescription dose was quartered by MU scaling for the experiments using the EBT3 films. Dose deliveries were performed via the dose delivery approaches as described in section 2.1.1. Similarly, the prescription dose was halved for the experiments using EBT-XD films for which only the proposed *tracking plus gating* dose delivery approach was used. As reference experiment, the prescribed dose (PD) was delivered in a static scenario (i.e. the target within the phantom was not moving).

2.1.7. Film dosimetry evaluation

Radiochromic films were scanned 24 h after irradiation with an Epson Expression 10 000XL flatbed scanner (Seiko Epson Corp, Nagano, Japan) with a resolution of 150 dpi. The digitized films were then processed by inhouse-developed software, which performs triple-channel dosimetry analysis with lateral corrections (Micke *et al* 2011, Li *et al* 2017). The film cassette insert creates indents in 3 corners of the film, which were used as landmarks to rigidly register all films to the static reference scenario. The resulting dose maps were then used to create dose difference maps with respect to the static reference measurement. The dose distribution maps were used to create line profiles through the center of the film in CC direction. The width difference of the profiles at 2, 6.25 and 8 Gy isolines were calculated with respect to the static reference. A local gamma analysis was done between the static reference scenario and the planned dose with 1%/1 mm and 2%/2 mm evaluation criteria. Next, local gamma analyses were done between the static reference scenario and the alternative motion-management scenarios using 1%/1 mm and 2%/2 mm evaluation criteria. Quantified dose $\leq 10\%$ of the PD were omitted for the gamma analyses to minimise film calibration uncertainties. The target coverage was analysed using dose area histograms (DAH).

2.2. Dosimetric in-silico study

In-silico experiments were conducted to quantify the dosimetric effects of cardiac motion and cardiac motion mitigation in three patient data sets (figure 3). IMRT plans for STAR treatment were created for these patients and used as input. Probability density functions were calculated and used as input for Monte Carlo simulations to estimate the effects of residual respiratory MLC-tracking errors, cardiac motion and cardiac gating on the radiation delivery.

2.2.1. Patient data and treatment planning

Patient data was retrospectively collected under the FAST-ART protocol (IRB reference: 20-519/C). Three anonymized patient data sets were used for the in-silico experiments. Artificial mid septal, basal lateral and

apical inferior gross target volumes (GTV) plus surrounding structures were delineated by an experienced radiation oncologist (as depicted in bottom left subfigure in figure 3). A 15-beam (with number of segments ranging from 68 to 71) IMRT plan (1×25 Gy) was then created in Monaco v.5.40.01, which was inspired by Knutson *et al* (2019). An isotropic PTV margin of 5 mm was used. The calculated maximum dose ranged from 37.1 to 37.8 Gy between patients. The treatment plan was calculated on a 1 mm dose grid. For plan calculation, an uncertainty level of 1% per control point was used.

2.2.2. Respiratory MLC-tracking characterization

The effect of residual respiratory MLC-tracking errors was characterized by calculating a normalized probability density function (PDF) with a single scenario using a Gaussian 3D kernel:

- Residual 3D. The kernel size was $5 \times 5 \times 5$ mm³ with a mean of 0 mm and standard deviation of 1 mm in all directions, in accordance with the guidelines of safe MLC-tracking implementation in radiotherapy (Keall *et al* 2021).

2.2.3. Cardiac motion characterization

The effect of cardiac motion was characterized by calculating a PDF based on three motion scenarios:

- Artificial 1D. Cardiac motion (70 bpm) in CC direction (\cos^4 , 10 mm peak-to-peak), which corresponds to one of the experimental motion scenarios.
- Artificial 3D. Cardiac motion (70 bpm) in CC (\cos^4 , 5 mm peak-to-peak), right-left (RL) (\cos^4 , 4 mm peak-to-peak) and AP (\cos^4 , 4 mm peak-to-peak) with motion amplitudes comparable with measured motion amplitudes in cardiac SBRT patients (Prusator *et al* 2021).
- Cine 3D. Cardiac motion (59 bpm) derived from *in vivo* data (Akdag *et al* 2021) in CC (9.2 mm peak-to-peak), RL (5.9 mm peak-to-peak) and AP (2.7 mm peak-to-peak) directions.

The cardiac motion traces were subtracted by their corresponding mean position and thereby centered around zero.

For all scenarios, a corresponding cardiac gated scenario was simulated. The zeroline was then considered the gating threshold and all positions below the zeroline (in each direction) were included in the simulation (see top right subfigure in figure 3). The histograms were calculated based on the described motion patterns in which the occurrence of the target was described on a 1x1 mm grid (as depicted in the top row in figure 3).

2.2.4. Motion-included dose accumulation

A GPU-based Monte Carlo Dose (GPUMCD) calculation engine was used to recalculate dose distributions of corresponding IMRT plans while taking the effect of the magnetic field of the Elekta Unity into account (Hissoiny *et al* 2011). For the Monte Carlo simulations, an effective dose uncertainty of 0.6% or higher per control point was reached on a 1 mm grid.

The motion patterns (described in section 2.2.3) were used to calculate relative isocenter shifts, which created plans with different isocenters as input for the simulation (Poulsen *et al* 2012). Each plan was assigned a weight w based on the motion PDF with $\sum_{i=1}^k w_i = 1$. The total resulting dose map is then the weighted sum of all simulated dose maps.

2.2.5. Dosimetric in-silico evaluation

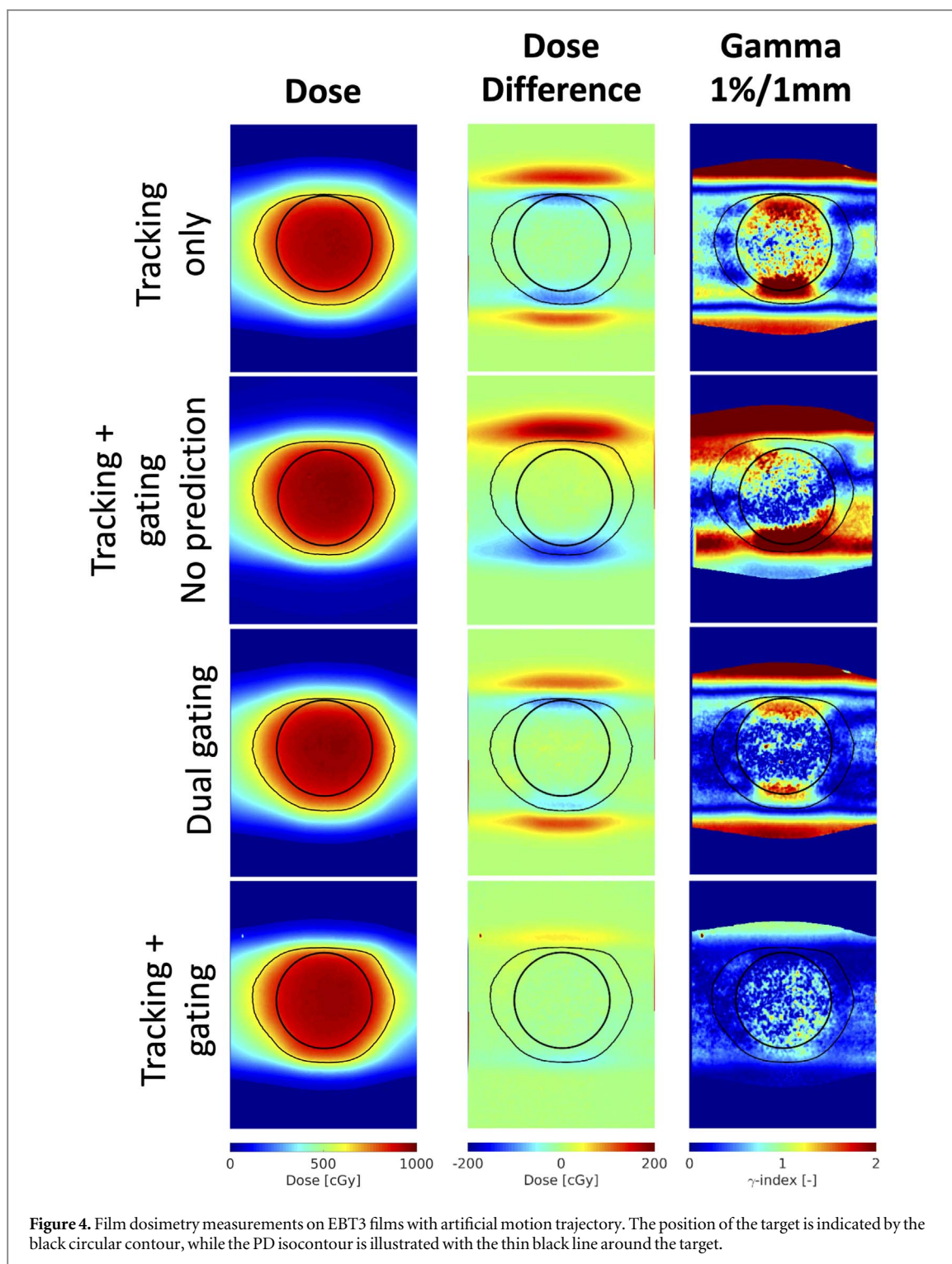
The motion-included accumulated dose maps were analyzed and dose volume histograms (DVHs) were extracted for the GTV and PTV and compared with the results from the static treatment plan.

3. Results

3.1. Phantom experiments on the MR-linac

3.1.1. System latencies

The estimated latency for MLC-tracking (τ_{MLC}) was 177.3 ± 1.9 ms. T_{signal} was 64.9 ± 1.1 ms. T_{proc} was 25.9 ± 3.1 ms. The necessary time to turn the beam on/off during gating (T_{gate}) was 35.0 ± 10.5 ms. The calculated latency for radiation delivery gating τ_{gate} was 125.8 ± 11.0 ms.

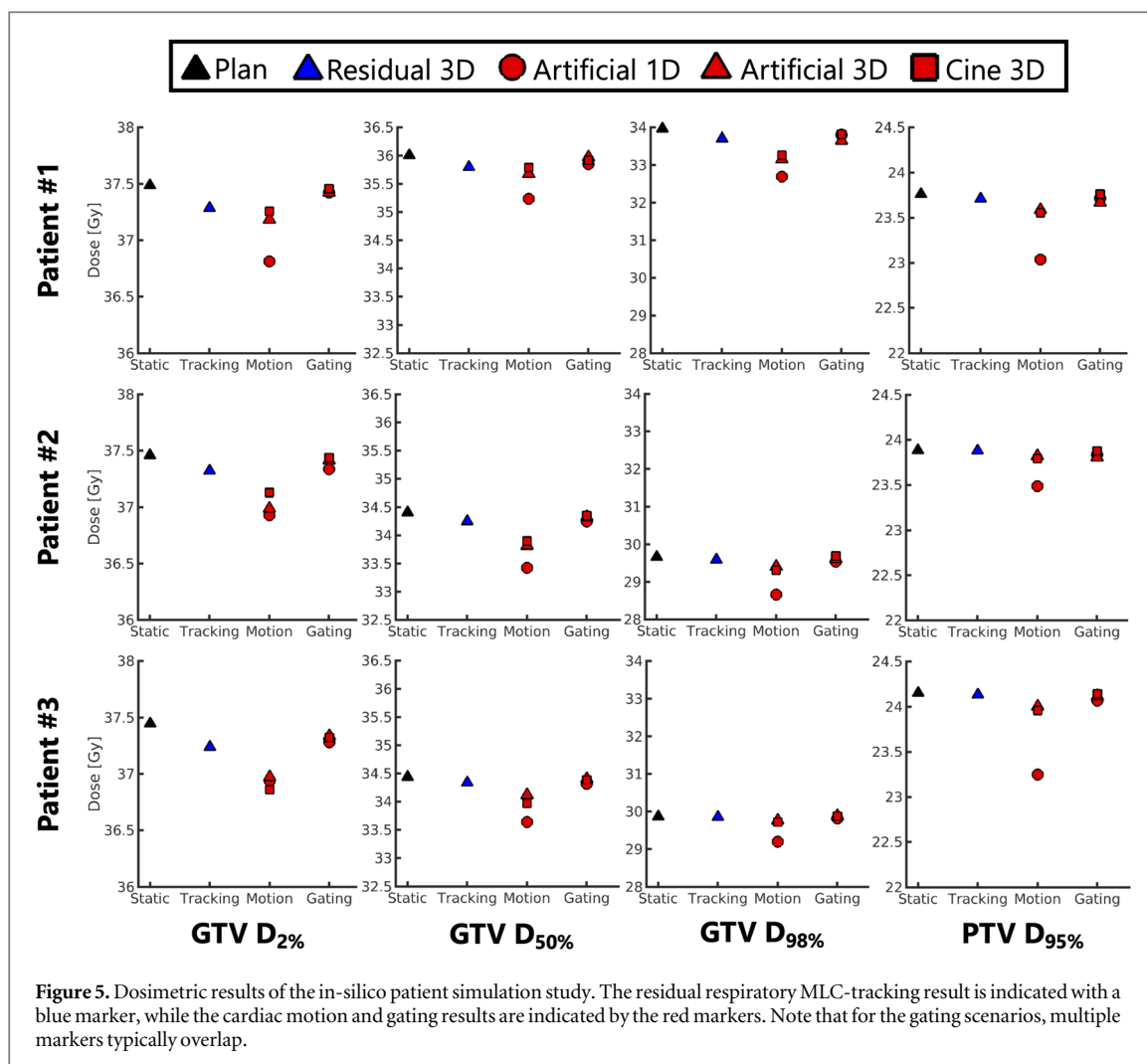


3.1.2. Plan delivery times and residual motion

The delivery time without active motion management would be 22.8 min. The radiation delivery during the tracking plus gating scenario (with and without prediction) for artificial (and subject-derived) cardiac motion had a duty cycle of 57% (57%), which would result in a scaled delivery time of 37.3 (37.3) min with 1.1 (1.4) mm residual motion (i.e. RMS target displacements within the gating window). With artificial (and subject-derived) cardiac motion, the duty cycle was decreased to 28.5% (28.5%) for the dual gating scenario, which would result in a prolonged total plan delivery time of 72 (72) min with 3.3 (3.4) mm residual motion.

3.1.3. Motion estimation accuracy

The artificial motion signal was used to determine the accuracy of the motion signal estimation. The MAE (RMSE) was 0.52 (0.66) mm for the total motion signal. The MAE (RSME) was 0.74 (0.92) mm for the cardiac motion component and 0.64 (0.78) mm for the respiratory motion component.



3.1.4. Film dosimetry

The static reference scenario was first compared with the pre-calculated IMRT plan and gamma pass rates of 77.3% and 95.2% were obtained with 1%/1 mm and 2%/2 mm evaluation criteria, respectively. Measured dose distribution maps, dose difference maps (with respect to the static reference) and gamma analysis maps (1%/1 mm) are shown in figure 4 for the artificial motion trajectory. The film dosimetry results for the subject-derived motion trajectory and EBT-XD films can be found in figure S2 and S3 in the supplement. Table 1 summarizes the quantitative dosimetric results of the proposed tracking plus gating motion management scenario and the alternative scenarios. The gamma pass rates and DAH of the tracking plus gating scenario were in close agreement with the static reference. The DAH of tracking plus gating without cardiac motion prediction was observed to be superior with respect to all other scenarios, but came with a maximum gamma pass rate (1%/1 mm) of 71.5% and dose differences (with respect to the static reference) with a maximum of +28.8% of the PD outside the GTV, while the maximum dose difference is limited to +9.6% of the PD for the tracking plus gating (with cardiac motion prediction) scenario.

3.1.5. Line profile widths

For the tracking and gating scenarios with artificial (and subject-derived) cardiac motion, the width differences were 0.7 (0.9), -0.3 (-0.5) and -0.7 (-1.0) mm, respectively. For the tracking-only case with artificial (and subject-derived) cardiac motion, the width differences were 4.2 (5.4), -1.7 (-2.2) and -3.9 (-5.3) mm, respectively. For the dual gating case with artificial (and subject-derived) cardiac motion, the width differences were 3.4 (3.4), -1.2 (-1.5) and -2.7 (-3.6) mm, respectively. For the tracking and gating without cardiac motion prediction for artificial (and subject-derived) cardiac motion, the width differences were 2.9 (2.5), -0.7 (-0.7) and -2.2 (-2.2) mm, respectively.

3.1.6. Dose area histogram

The $D_{2\%}$ and $D_{50\%}$ levels agreed within -2.4% to $+0.8\%$ in all scenarios with respect to the static reference.

Table 1. Dose area histogram and gamma pass rates for the film dosimetry experiments.

	DAH Target			Gamma pass rates ($\geq 10\%$ PD)	
	$D_{2\%}$ [Gy]	$D_{50\%}$ [Gy]	$D_{98\%}$ [Gy]	1% / 1 mm (%)	2% / 2 mm (%)
Static (EBT3)	9.53	9.24	8.4	—	—
Tracking-only					
Artificial	9.41	9.07	7.58	57.9	90.3
Subject-derived	9.41	9.02	7.20	42.6	79.8
Dual gating					
Artificial	9.57	9.19	7.64	73.3	95.9
Subject-derived	9.36	9.02	7.52	56.9	89.2
Tracking + gating w/o predictor					
Artificial	9.61	9.29	8.31	43.4	80.8
Subject-derived	9.52	9.18	8.31	71.5	89.1
Tracking + gating					
Artificial	9.47	9.18	8.19	98.8	100.0
Subject-derived	9.48	9.20	8.19	99.3	100.0
Static (EBT-XD)	18.4	17.7	15.7	—	—
Tracking + gating (EBT-XD)					
Artificial	18.1	17.5	15.4	94.3	99.7

The main differences in target coverage were seen in the near minimum dose ($D_{98\%}$). When cardiac motion mitigation was omitted, the minimum dose decreased by 9.8% and 14.3% for artificial and subject-derived motion, respectively, with respect to the static reference. For the dual gating scenario, the minimum dose was then decreased by 9.0% and 10.5% for artificial and subject-derived motion, respectively. For tracking plus gating, without prediction of cardiac motion, the minimum dose was decreased by 1.1%, while a decrease of 2.5% was observed with cardiac motion prediction.

3.1.7. Gamma analysis

Figure 4 shows examples of 1%/1 mm gamma analysis maps relative to the static reference. The tracking plus gating scenario yields (1%/1 mm) gamma pass rates as high as 99.3%. From the alternative scenarios, dual gating yields the highest gamma pass rate of 73.3%. When cardiac motion prediction was omitted in the tracking plus gating scenario, a decrease of 55.4% points was observed for the artificial cardiac motion trace, while the decrease was limited to 27.8% points for the subject-derived cardiac motion trace.

3.2. In silico experiments

The target DVH points from the Monte Carlo dose simulations are shown in figure 5 for the residual respiratory MLC-tracking, cardiac motion and cardiac gating scenarios.

3.4. Respiratory MLC-tracking

For all patients, the GTV $D_{2\%}$ dose deviated in a range of -1.3% to -0.6% with respect to the calculated planned dose. Similarly, the GTV $D_{50\%}$ dose deviated in a range of -0.3% – -0.2% and the GTV $D_{98\%}$ dose deviated between -0.9 and $+0.1\%$ for all patients. The PTV $D_{95\%}$ dose deviated by -0.3 to $+0.1\%$ for all patients.

3.5. Cardiac motion and cardiac gating

For all patients, cardiac motion deviated GTV $D_{2\%}$ dose between -1.8% and -0.6% . Cardiac gating limited the GTV $D_{2\%}$ dose deviation to -0.4% or better. Cardiac motion deviated the GTV $D_{50\%}$ in a range of -2.8 – -0.6% for all patients. With cardiac gating, GTV $D_{50\%}$ deviated in a range of -0.4% and -0.1% . The main differences in GTV dose were observed at the (near) minimum dose level. Cardiac motion deviated GTV $D_{98\%}$ dose between -3.7 and -0.3% for all patients. Cardiac gating reduced the deviation in GTV $D_{98\%}$ dose in the range from -0.9% to $+0.1\%$ for all patients. Cardiac motion deviated PTV $D_{95\%}$ dose between -3.8% and -0.2% for all patients. Cardiac gating reduced the deviation of the PTV $D_{95\%}$ dose to -0.4 – 0.0% for all patients.

4. Discussion

To our knowledge, this is the first study in which real-time cardiorespiratory motion mitigation is demonstrated for online MRI-guided STAR on the MR-linac. Cardiac motion was successfully mitigated using gating, which was demonstrated in the phantom and in-silico experiments. In addition, the possibility to mitigate cardiac and

respiratory motion simultaneously during the radiation delivery was shown experimentally by combining cardiac gating with respiratory MLC-tracking.

A real-time 2D cine MRI bSSFP sequence was developed with a 13 Hz framerate with sufficient contrast for cardiorespiratory motion detection. The high motion frequency of the heart required a motion mitigation infrastructure that operates in real-time. The sequence was used for imaging of the phantom, and previously also for imaging healthy volunteers (Akdag *et al* 2021). The motion was quantified in real-time with in-house developed C++ software with sub-millimeter agreement. Therefore, it was possible to acquire a cardiac motion signal that could be used as input for cardiac motion-mitigated radiation delivery.

The MLC-tracking latency (τ_{MLC}) was measured to be 177.3 ± 1.9 ms, while the gating latency (τ_{gate}) was calculated to be 125.8 ± 11.0 ms. If not accounted for, these system latencies would cause the linear accelerator to act on outdated target positions. The previously developed prediction model for respiratory motion (Uijtewaal *et al* 2021) was accommodated for cardiac motion prediction, thus allowing us to gate the radiation delivery within a single heartbeat in real-time.

Our film dosimetry setup showed excellent agreement with the planned dose for the static scenario. For the tracking plus gating scenario, the dosimetric film results showed that the dose difference with respect to the static reference was small and returned a gamma pass rate of 99%. Residual motion decreased with 70% for the artificial motion pattern and 68% for the subject-derived motion pattern with respect to the tracking-only scenario, thus limiting the dosimetric effects of residual motion.

Our MR-linac STAR plan had a delivery time of 22.8 min without gating when scaled to the full 25 Gy prescription. MLC-tracking achieved a 100% duty cycle for respiratory motion mitigation. The radiation delivery time was increased to 37.3 min when combining MLC-tracking with cardiac gating. The radiation delivery time was extensively prolonged to 72 min in the dual gating case as the respiratory beam gating had a duty cycle of 50%. In a clinical setting, this would likely be unacceptable due to decreased patient comfort and throughput.

Alternative motion mitigation scenarios were compared to the tracking plus gating scenario. First, the effect of cardiac gating was isolated by only applying respiratory motion tracking. The dose increased in the area surrounding the GTV and decreased in the GTV with respect to the static reference. The width difference of the line profile with respect to the static reference supports this observation. The decreased dose conformality highlighted the advantages of mitigating cardiac motion. Second, the dual gating dose delivery scenario was an approach to mitigate cardiac and respiratory motion by gating the radiation delivery based on both the cardiac and respiratory motion components in parallel. Dose was only delivered when both motion signals were within their respective gating windows. This delivery scenario is superior to the tracking-only scenario regarding dose conformality, but is inferior to tracking plus gating in the same regard. The respiratory motion component had a generous gating window of 10 mm contributing to a less conformal dose delivery due to residual motion. Decreasing the gating window would decrease the residual motion, but would simultaneously increase the delivery time even further. The decreased conformality was indicated by the GTV $D_{98\%}$, line profile width differences and gamma pass rates. Third, the tracking and gating scenario was performed without cardiac motion prediction to isolate the effect of cardiac motion prediction. A slightly higher dose level was obtained within the target, which showed that the target coverage was not degraded when omitting the cardiac motion prediction. However, the dose difference map showed clear dose differences beyond the cranial and caudal edges of the target. The hotspot beyond the cranial edge of the target showed that unwanted dose deposition would occur in healthy tissue. In addition, the gamma analysis revealed a considerably lower pass rate with respect to the scenario with cardiac motion prediction. When omitting cardiac motion prediction, a systematic beam alignment error was introduced resulting in a small performance degradation relative to the tracking-only case. Given our cardiac motion traces (59–70 bpm), the gating latency had only a moderate effect. However, it is expected that for faster heartbeats or more irregular cardiac motion, the impact of latency on the gating permanence is greater.

Additional in-silico experiments were performed to isolate the dosimetric effects of residual respiratory MLC-tracking, cardiac motion and cardiac motion mitigation during STAR in more realistic anatomies. The selected cardiac motion traces were not accurately representative of typical STAR patients, but it was important to show that a wider variety of motion amplitudes can be mitigated for improved dosimetric results. The respiratory MLC-tracking simulations showed that the deviations of the resulting DVH points are acceptably small to omit from the cardiac motion and gating in-silico experiments.

Our simulations confirmed that a higher dose conformality can be achieved when the radiation delivery is limited to a pre-defined cardiac phase. Given our selection of artificial and measured cardiac motion traces, a dose loss of up to of 3.7% (GTV $D_{98\%}$) and 3.8% (PTV $D_{95\%}$) can be prevented compared to a static reference plan, thus indicating that an improved target coverage can be achieved with cardiac motion mitigation. The results of the in-silico experiments thus confirm the results of the phantom experiments. In contrast to the phantom experiments, the in-silico experiments regarding cardiac motion and gating were constructed such

that the whole plan was delivered at each isocenter based on cardiac motion only. The residual error assumed in the in-silico experiments for respiratory MLC-tracking were based on guidelines on safe clinical implementation of MLC-tracking. The interplay of treatment delivery and cardiorespiratory motion mitigation was therefore ignored.

In this study, we set out to demonstrate the capability of the Elekta Unity MR-linac to mitigate cardiorespiratory motion by simultaneous cardiac gated radiation delivery and respiratory MLC-tracking for the benefit of future STAR treatments. While we managed to demonstrate the potential of the Unity MR-linac with phantom and in-silico experiments, it is also acknowledged that additional developments are needed before clinical translation.

A 1D CC motion signal was used to mimic cardiorespiratory motion in accordance with the capabilities of our motion phantom. In reality, cardiac and respiratory motion are not typically aligned (Roujol *et al* 2013). More complex and realistic cardiorespiratory phantoms are desirable for future studies to analyse 3D motion mitigation.

Further research is required to develop robust imaging strategies for simultaneous tracking and gating motion management. In this study, MRI-guidance was based on a balanced cine imaging sequence. Balanced imaging sequences are highly sensitive to cardiac implantable electronic devices (CIEDs), which are typically present in VT patients, as they cause severe off-resonance artifacts (Löbe *et al* 2020). Several techniques are available to minimize CIED-induced image artifacts (Hong *et al* 2020). However, MRI developments regarding CIEDs falls out of the scope of this paper.

In this study, an imaging frequency of 13 Hz was used for cardiac motion quantification. The artificial motion signal of the phantom experiments had a heart frequency of 70 bpm and the *in vivo* cardiac signal was from a healthy volunteer with an average heart rate of 59 bpm. For higher heart rates, the quality of the cardiac motion signal could deteriorate at our currently used imaging frequency of 13 Hz. Image acceleration for accurate cardiac motion estimation should therefore be a separate research aspect for MRI-guided STAR, while complying with safety limits concerning MR imaging of patients with a CIED (Horwood *et al* 2016, Maass *et al* 2018).

For target position estimation, a 2D imaging approach was used for 1D motion mitigation in a phantom setup. The position of the target was estimated by normalized cross-correlation. The motion estimation approach was sufficient to demonstrate the cardiorespiratory motion mitigation capabilities on the Unity MR-linac using a phantom setup. Motion estimation becomes more challenging when the position of the target within the heart has to be estimated.

Feasibility studies were conducted in healthy volunteers to retrospectively estimate the position of a localized region of interest within the left ventricle using template matching on a single slice 2D cine MRI in real-time. Template matching works reasonably well in healthy volunteers, but the effect of tissue deformation on the position estimation was not included in this registration approach (Akdag *et al* 2021). In the research domain, a template matching algorithm was reported in which real-time acquired orthogonal 2D cardiac cine MRI were matched to a 3D template to estimate the motion of the LA with a mean error of 3.2 mm in 3D phantom data and 1–2 mm in each orthogonal direction in 2D volunteer data (Ipsen *et al* 2016). This study focused on position estimation accuracy only and was therefore only tested on healthy volunteers. A similar motion mitigation approach was reported for lung radiotherapy (Paganelli *et al* 2018). An extensive study was conducted for motion characterization of the left atrium. Here, a stack of 2D cine MRI slices were used to quantify the motion of the left atrium in healthy volunteers and atrial fibrillation patients (Lydiard *et al* 2021). Motion estimation techniques by only using *k*-space data (Huttinga *et al* 2021) could also pose as a potential solution for real-time motion compensation in 3D during MRI-guided radiotherapy.

However, further research on more accurate motion compensation techniques was beyond the scope of this paper. It is essential to conduct future research studies in which robust imaging approaches will be developed together with image processing/registration approaches to achieve accurate motion compensation, especially in the presence of CIEDs.

The quantified positions of the target were deconvoluted using a prospective linear Kalman filter, optimised for periodic respiratory motion. Kalman filters optimised for a wider range of motion scenarios were outside the scope of this manuscript.

The predictor model was used on motion traces with a limited amount of variability. The performance of the predictor model was extensively tested by Uijtewaal *et al* (2020) for respiratory motion traces. The predicted positions were returned with sub-millimeter accuracy while accuracy degradation would be limited with increased variability in the motion signal by re-training the predictor model. Further research on the performance of the predictor model on varying cardiac motion traces should be conducted in future studies.

The cardiac gating approach, as demonstrated in this study, reduced the duty cycle to 57%, while obtaining a gamma pass rate of minimally 98.8%. To maintain a potential duty cycle of 100%, purely MLC-tracking based cardiorespiratory motion mitigation could be explored in future studies (Lydiard *et al* 2018).

Recently, a cardiac synchronized VMAT delivery was proposed on a C-arm linac (Poon *et al* 2020). Here, the proposed cardiac synchronized treatment approach focused on delivering the radiation in the quiescent phase of the cardiac cycle, based on an electrocardiography (ECG) signal, to minimize the effect of motion on the dose delivery. C-arm and robotic linac lack the possibility to directly visualize the 3D position of the cardiac target for real-time online guidance of radiotherapy. ECGs are commonly used in the field of CMR for MR imaging in a pre-defined cardiac phase. Nevertheless, while the ECG is able to return a cardiac signal in real-time, it is not able to provide information about the absolute position of the target. For the first STAR patient treated on an MR-linac, respiratory gating was performed by cine tracking of extra-cardiac structures (i.e. liver dome, diaphragm and esophagus) surrogates with a frame rate of 4 Hz (Mayinger *et al* 2020).

5. Conclusion

Real-time cardiorespiratory motion management on the 1.5 T MR-linac greatly reduces motion-induced dosimetric uncertainty. Further research and development is warranted for potential future use in STAR.

Acknowledgments

Martin F. Fast and Prescilla Uijtewaal acknowledge funding by the Dutch Research Council (NWO) through project no. 17 515 (BREATHE EASY).

MLC-tracking research at UMC Utrecht is performed under a research agreement with Elekta AB. Peter Woodhead is a part-time contractor for Elekta.

ORCID iDs

O Akdag  <https://orcid.org/0000-0003-4730-7635>

P T S Borman  <https://orcid.org/0000-0003-4153-2241>

S Mandija  <https://orcid.org/0000-0002-4612-5509>

J J C Verhoeff  <https://orcid.org/0000-0001-9673-0793>

M F Fast  <https://orcid.org/0000-0001-9107-4627>

References

- Akdag O, Mandija S, Borman P T, Alberts E and Fast M F 2021 Feasibility of free breathing real-time cine-MRI for MR-guided cardiac radioablation on the Unity MR-linac *Proc. Intl. Soc. Mag. Reson. Med.* **29** 4014
- Aliot E M *et al* 2009 EHRA/HRS expert consensus on catheter ablation of ventricular arrhythmias *Heart Rhythm* **6** 886–933
- Borman P T S, Tijssen R H N, Bos C, Moonen C T W, Raaymakers B W and Glitzner M 2018 Characterization of imaging latency for real-time MRI-guided radiotherapy *Phys. Med. Biol.* **63** 155023
- Calkins H *et al* 2000 Catheter ablation of ventricular tachycardia in patients with structural heart disease using cooled radiofrequency energy *J. Am. College Cardiol.* **35** 1905–14
- Cuculich P S *et al* 2017 Noninvasive cardiac radiation for ablation of ventricular tachycardia *New Engl. J. Med.* **377** 2325–36
- Curtis A D and Cheng H M 2020 Primer and historical review on rapid cardiac cine MRI *J. Magn. Reson. Imaging* **55** 373–388
- Cvek J *et al* 2014 Cardiac radiosurgery for malignant ventricular tachycardia *Cureus* **6** e190
- Hissoiny S, Raaijmakers A J E, Ozell B, Després P and Raaymakers B W 2011 Fast dose calculation in magnetic fields with GPUMCD *Phys. Med. Biol.* **56** 5119–29
- Hong S, Hong K, Culver A E, Pathrose A, Allen B D, Wilcox J E, Lee D C and Kim D 2020 Highly accelerated real-time free-breathing cine cmr for patients with a cardiac implantable electronic device *Acad. Radiol.* **28** 1779–86
- Horwood L, Attili A, Luba F, Ibrahim E S H, Parmar H, Stojanovska J, Gadoth-Goodman S, Fette C, Oral H and Bogun F 2016 Magnetic resonance imaging in patients with cardiac implanted electronic devices: focus on contraindications to magnetic resonance imaging protocols *Europace* **19** 812–7
- Huttinga N R F, Bruijnen T, Van den Berg C A T and Sbrizzi A 2022 Real-time non-rigid 3D respiratory motion estimation for MR-guided radiotherapy using MR-MOTUS *IEEE Trans. Med. Imaging* **41** 332–46
- Ipsen S, Blanck O, Lowther N J, Liney G P, Rai R, Bode F, Dunst J, Schweikard A and Keall P J 2016 Towards real-time MRI-guided 3D localization of deforming targets for non-invasive cardiac radiosurgery *Phys. Med. Biol.* **61** 7848–63
- Keall P J *et al* 2006 The management of respiratory motion in radiation oncology report of AAPM Task Group 76a): Respiratory motion in radiation oncology *Med. Phys.* **33** 3874–900
- Keall P J *et al* 2021 AAPM Task Group 264: the safe clinical implementation of MLC tracking in radiotherapy *Med. Phys.* **48** e44–e64
- Kramer C M, Barkhausen J, Bucciarelli-Ducci C, Flamm S D, Kim R J and Nagel E 2020 Standardized cardiovascular magnetic resonance imaging (CMR) protocols: 2020 update *J. Cardiovascular Magnetic Resonance* **22** 1–18
- Krauss A, Nill S and Oelfke U 2011 The comparative performance of four respiratory motion predictors for real-time tumour tracking *Phys. Med. Biol.* **56** 5303–17
- Löbe S *et al* 2020 Evaluation of the right heart using cardiovascular magnetic resonance imaging in patients with cardiac devices *Int. J. Cardiol.* **316** 266–71
- Lee S E, Nguyen C, Xie Y, Deng Z, Zhou Z, Li D and Chang H J 2019 Recent advances in cardiac magnetic resonance imaging *Korean Circ. J.* **49** 146–59

- Li Y, Chen L, Zhu J and Liu X 2017 The combination of the error correction methods of GAFCHROMIC EBT3 film *PLoS One* **12** e0181958
- Liu Z, Yasmeh B, Verdick C, Rajsheker S, Barone A and Costea A 2019 New trends in high risk ventricular tachycardia catheter ablation *J. Cardiovascular Dis. Res.* **10** 01–8
- Lydiard P S, Blanck O, Hugo G, O'Brien R and Keall P 2021 A review of cardiac radioablation (cr) for arrhythmias: procedures, technology, and future opportunities *Int. J. Radiat. Oncol. Biol. Phys.* **109** 783–800
- Lydiard S, Caillet V, Ipsen S, O'Brien R, Blanck O, Poulsen P R, Booth J and Keall P 2018 Investigating multi-leaf collimator tracking in stereotactic arrhythmic radioablation (STAR) treatments for atrial fibrillation *Phys. Med. Biol.* **63** 195008
- Lydiard S, Pontré B, Lowe B S, Ball H, Sasso G and Keall P 2021 Cardiac radioablation for atrial fibrillation: target motion characterization and treatment delivery considerations *Med. Phys.* **48** 931–41
- Maass A H, Hemels M E W and Allaart C P 2018 Magnetic resonance imaging in patients with cardiac implantable electronic devices *Netherlands Heart J.* **26** 584–90
- Marchlinski F E, Callans D J, Gottlieb C D and Zado E 2000 Linear ablation lesions for control of unmappable ventricular tachycardia in patients with ischemic and nonischemic cardiomyopathy *Circulation* **101** 1288–96
- Mayinger M et al 2020 First magnetic resonance imaging-guided cardiac radioablation of sustained ventricular tachycardia *Radiother. Oncol.* **152** 203–7
- Micke A, Lewis D F and Yu X 2011 Multichannel film dosimetry with nonuniformity correction: multichannel film dosimetry with nonuniformity correction *Med. Phys.* **38** 2523–34
- Paganelli C, Lee D, Kipritidis J, Whelan B, Greer P B, Baroni G, Riboldi M and Keall P 2018 Feasibility study on 3D image reconstruction from 2D orthogonal cine-MRI for MRI-guided radiotherapy *J. Med. Imaging Radiat. Oncol.* **62** 389–400
- Poon J, Kohli K, Deyell M W, Schellenberg D, Reinsberg S, Teke T and Thomas S 2020 Technical note: cardiac synchronized volumetric modulated arc therapy for stereotactic arrhythmia radioablation Proof of principle *Med. Phys.* **47** 3567–72
- Poulsen P R, Schmidt M L, Keall P, Worm E S, Fledelius W and Hoffmann L 2012 A method of dose reconstruction for moving targets compatible with dynamic treatments: dose reconstruction for moving targets *Med. Phys.* **39** 6237–46
- Prusator M T, Samson P, Cammin J, Robinson C, Cuculich P, Knutson N C, Goddu S M, Moore K and Hugo G D 2021 Evaluation of motion compensation methods for noninvasive cardiac radioablation of ventricular tachycardia *Int. J. Radiat. Oncol. Biol. Phys.* **111** 1023–32
- Robinson C G et al 2019 Phase I/II trial of electrophysiology-guided noninvasive cardiac radioablation for ventricular tachycardia *Circulation* **139** 313–21
- Roujol S, Anter E, Josephson M E and Nezafat R 2013 Characterization of respiratory and cardiac motion from electro-anatomical mapping data for improved fusion of mri to left ventricular electrograms *PLoS One* **8** e78852
- Scholz E P, Seidensaal K, Naumann P, André F, Katus H A and Debus J 2019 Risen from the dead: Cardiac stereotactic ablative radiotherapy as last rescue in a patient with refractory ventricular fibrillation storm *Heart Rhythm Case Rep.* **5** 329–32
- Sharp A J, Mak R and Zei P C 2019 Noninvasive cardiac radioablation for ventricular arrhythmias *Curr. Cardiovasc. Risk Rep.* **13** 1–10
- Soejima K, Suzuki M, Maisel W H, Brunckhorst C B, Delacretaz E, Blier L, Tung S, Khan H and Stevenson W G 2001 Catheter ablation in patients with multiple and unstable ventricular tachycardias after myocardial infarction: Short ablation lines guided by reentry circuit isthmuses and sinus rhythm mapping *Circulation* **104** 664–9
- Spincemaille P, Nguyen T D, Prince M R and Wang Y 2008 Kalman filtering for real-time navigator processing *Magn. Reson. Med.* **60** 158–68
- Uijtewaal P, Borman P T, Woodhead P L, Hackett S L, Raaymakers B W and Fast M F 2021 Dosimetric evaluation of MRI-guided multi-leaf collimator tracking and trailing for lung stereotactic body radiation therapy *Med. Phys.* **48** 1520–32
- van der Ree M H et al 2020 Cardiac radioablation—a systematic review *Heart Rhythm* **17** 1381–92
- Zei P C and Soltys S 2017 Ablative radiotherapy as a noninvasive alternative to catheter ablation for cardiac arrhythmias *Curr. Cardiol. Rep.* **19** 2–9